Available online at www.sciencedirect.com
SCIENCE DIRECT®
Journal of Solid State Chemistry 178 (2005) 1212–1220
JOURNAL OF SOLID STATE CHEMISTRY
www.elsevier.com/locate/jssc

Two aluminotriphosphates with closely related intersecting tunnel structures involving tetrahedral "AlP" chains and layers: $A Al_3(P_3O_{10})_2$, A = Rb, Cs

J. Lesage, A. Guesdon*, B. Raveau

Laboratoire CRISMAT (UMR 6508), CNRS—ENSICAEN, 6 Bd Maréchal Juin, 14050 Caen Cedex, France

Received 17 November 2004; accepted 13 January 2005

Abstract

Two new aluminotriphosphates, $RbAl_3(P_3O_{10})_2$ and $CsAl_3(P_3O_{10})_2$, were synthesized by solid-state reaction. They crystallize in non-centrosymmetric space groups: $C222_1$ with $a = 9.8757(7)$ Å, $b = 12.8854(10)$ Å, $c = 11.9192(7)$ Å, ($Z = 4$) for $RbAl_3(P_3O_{10})_2$ and $C2ce$ with $a = 10.0048(7)$ Å, $b = 13.3008(10)$ Å, $c = 12.1698(7)$ Å, ($Z = 4$) for $CsAl_3(P_3O_{10})_2$. Their 3D frameworks, built up of corner sharing P_3O_{10} groups, AlO_4 tetrahedra and AlO_6 octahedra, exhibit several remarkable features. The AlO_4 tetrahedra and P_3O_{10} groups are directly associated through the corners, forming helical columns in the Rb-phase and "helicoid" layers in the Cs-phase. The simultaneous presence of AlO_4 and AlO_6 species, rather rare in phosphates, leads to the formation of closely related $[Al_3P_6O_{24}]_\infty$ layers in both structures, which differ by their stacking mode. The presence of intersecting tunnels running along $\langle 110 \rangle$ and [001] directions, with Rb^+ and Cs^+ sitting at the intersections, shows the opened character of these two structures.

Keywords: Single crystal; X-ray diffraction; Structure determination; Tunnel structure; Three-dimensional host lattice; Aluminium triphosphate

1. Introduction

The great ability of aluminium to accommodate several coordinations—tetrahedral, octahedral and even bipyramidal—involves that its association with elements that can only adopt a tetrahedral coordination, like silicon or phosphorus, allows the formation of opened frameworks in oxides. Consequently, aluminosilicates and aluminophosphates have been the purpose of numerous studies in view of various applications in the fields of catalysis and separation [1–4 and references therein]. Compared to aluminosilicates, aluminophosphates are much less numerous if one except the organically templated aluminophosphates, the hydroxyphosphates and hydrates, and they have the advantage to be synthesized at lower temperature. Moreover, several studies of monazites and apatites [5,6] show that phosphates can also constitute a valuable crystalline matrix for the storage of nuclear wastes, suggesting that the exploration of aluminophosphates with an opened framework, susceptible to accommodate radiative cations like cesium, is of great importance.

Our previous investigation of the Cs–Al–P–O system, which led to the triphosphate $Cs_2AlP_3O_{10}$ [7], was based on the above considerations of the potential of aluminophosphate frameworks. In the latter aluminophosphate, aluminium behaves as a "normal" cation and exhibits the octahedral coordination, so that in this layer structure, the triphosphate groups are interconnected through AlO_6 octahedra. At this point of the knowledge of the Cs–Al–P–O system, it is vital to consider the possibility to introduce tetrahedral species concomitantly with the PO_4 tetrahedra, in order to form mixed tetrahedral frameworks like in zeolites. The recent synthesis of the aluminophosphate

*Corresponding author. Fax: +33 2 31 95 16 00.
E-mail address: anne.guesdon@ensicaen.fr (A. Guesdon).

0022-4596/$ - see front matter © 2005 Elsevier Inc. All rights reserved.
doi:10.1016/j.jssc.2005.01.012

$NaCs_2Al(PO_4)_2$ [8], whose structure consists of vertex-sharing AlO_4 and PO_4 tetrahedra forming a 3D $[AlP_2O_8]_\infty$ framework, suggests that such a feature appears for smaller P/Al molar ratio, i.e., 2 instead of 3 for the first $Cs_2AlP_3O_{10}$ phosphate. We have revisited the systems Cs–Al–P–O and Rb–Al–P–O, involving P/Al ratio $\leqslant 2$. We describe herein two new aluminophosphates, $RbAl_3(P_3O_{10})_2$ and $CsAl_3(P_3O_{10})_2$, which exhibit closely related original intersecting tunnel structures, both built up of corner-sharing AlO_6 octahedra, AlO_4 tetrahedra and triphosphate groups P_3O_{10} and we emphasize the great ability of AlO_4 and P_3O_{10} units to share corners, forming helical columns in the Rb-phase and "helicoid" layers in the Cs-phase.

2. Experimental

2.1. Synthesis and crystal growth

The single crystals used for the structures determinations of $RbAl_3(P_3O_{10})_2$ and $CsAl_3(P_3O_{10})_2$ were extracted from preparations synthesized in two steps at the stoichiometric compositions (Rb (Cs):Al:P = 1:3:6). The first step consisted in heating up at approximately 770 K during a few hours in air the beforehand finely ground mixture of Al_2O_3 (Carlo Erba 99%), $(NH_4)_2HPO_4$ (Prolabo Normapur 99.5%) and ANO_3 (A = Rb, Cs; Chempur 99.9%) placed in a platinum crucible. The so obtained whitish powders were then finely ground again in an agate mortar. In a second step, the cesium aluminium mixture was placed in a platinum crucible and heated up during 24 h at 1173 K, then slowly cooled down to 1093 K for 48 h. For the rubidium–aluminium phosphate, the powder was placed in a silica tube, which was evacuated and sealed. It was heated up at 1123 K for 20 h then cooled at 1 K/h down to 1103 K and at 10 K/h down to 1003 K.

Attempts to synthesize these two aluminophosphates in the form of polycrystalline samples confirmed the formation of the latter as the major phase. Nevertheless, careful X-ray powder characterization revealed the presence in the samples of minor impurity phases.

2.2. Powder X-ray diffraction studies

The X-ray powder diffraction patterns of these triphosphates were registered with a PHILIPS PW 1830 diffractometer using the Cu$K\alpha$ radiation. For $RbAl_3(P_3O_{10})_2$, the 2θ angle ranged from 5° to 100° with a step of 0.02° and 9.8 s per step. For $CsAl_3(P_3O_{10})_2$, the 2θ angle ranged from 5° to 85° with a step of 0.02° and with 12 s per step. The cell parameters were refined in pattern matching mode with the program FullProf [9]. Most of the diffraction peaks were indexed in orthorhombic cells compatible with those determined from the single crystals studies, with $a = 10.0214(5)$ Å, $b = 13.3292(7)$ Å, $c = 12.1873(6)$ Å for the cesium phase and $a = 9.8849(3)$ Å, $b = 12.9032(4)$ Å, $c = 11.9279(4)$ Å for the rubidium phase. However, these refinements revealed the existence of a few non-indexed peaks, corresponding to the presence of at least one secondary unidentified phase.

2.3. Crystal studies

The semi-quantitative analyses of the colourless crystals extracted from the two preparations were performed with an OXFORD 6650 microprobe mounted on a PHILIPS XL30 FEG scanning electron microscope. The obtained cationic compositions were in agreement with the expected theoretical values of "10:30:60", respectively, for the alkali, metallic and phosphorus cations.

Several crystals were then optically selected to be tested. The dimension of the two single crystals that were chosen for the structure determinations and refinements are reported in Table 1. The data were collected with a Bruker-Nonius Kappa CCD four-circle diffractometer using the Mo$K\alpha$ radiation, equipped with a bidimensional CCD detector fixed at a distance of 34 mm from the crystals. Different strategies using φ and ω scans were determined, according to the size of the crystals (Table 1). The cell parameters reported in Table 1 were accurately determined from the whole registered frames. Data were reduced and corrected for Lorentz and polarization effects with the EvalCCD package [10]. Structure determinations and refinements for the two compounds were performed with the JANA2000 program [11].

For the rubidium phosphate, the observed systematic absences $hkl : h + k = 2n + 1$ and $00l : l = 2n + 1$ correspond to the non-centrosymmetric space group $C222_1$ (no. 20). The structure of $RbAl_3(P_3O_{10})_2$ was determined using the heavy atom method and then successive difference Fourier synthesis and Fourier synthesis. Absorption and secondary extinction effects corrections were applied. The refinement of the atomic coordinates and of the anisotropic thermal parameters of all atoms led to the reliability factors $R = 0.0371$ and $R_w = 0.0324$ (Table 1) and to the atomic parameters listed in Table 2a. The value of Flack parameter was $-0.004(9)$, confirming that the crystal was not twined by inversion. Note that, as expected, the solution corresponding to the enantiomorphic structure led to higher reliability factors ($R = 0.0772$ and $R_w = 0.0954$).

Two other crystals of this phosphate have been studied in order to check the possible existence of a crystal presenting the enantiomorphic structure. They both have the same structure than the first one, with Flack parameters of $-0.002(13)$ and 0.032(8), respectively.

Table 1
Summary of crystal data, intensity measurements and structure refinement parameters for $AAl_3(P_3O_{10})_2$ single crystals (A = Rb, Cs)

	$RbAl_3(P_3O_{10})_2$	$CsAl_3(P_3O_{10})_2$
1—*Crystal data*		
Crystal dimensions (mm^3)	$0.09 \times 0.05 \times 0.045$	$0.06 \times 0.09 \times 0.20$
Space group	$C222_1$ (# 20)	$C2ce$ (# 41)
Cell dimensions	$a = 9.8757(7)$ Å	$a = 10.0048(7)$ Å
	$b = 12.8854(10)$ Å	$b = 13.3008(10)$ Å
	$c = 11.9192(7)$ Å	$c = 12.1698(7)$ Å
Volume	1516.75(18) $Å^3$	1619.46(19) $Å^3$
Z	4	4
Formula weight ($g\,mol^{-1}$)	672.2	719.7
ρ_{calc} ($g\,cm^{-3}$)	2.94	2.95
2—*Intensity measurements*		
λ(Mo$K\alpha$)	0.71069 Å	0.71069 Å
	φ and ω scans	φ and ω scans
	0.5°/frame	0.5°/frame
Scan strategies	120 s/°	60 s/°
	2 iterations	2 iterations
Crystal-detector distance	Dx = 34 mm	Dx = 34 mm
θ range for data collection	$6.03° \leqslant \theta \leqslant 34.95°$	$5.89° \leqslant \theta \leqslant 39.94°$
	$-15 \leqslant h \leqslant 12$	$-18 \leqslant h \leqslant 16$
Limiting indices	$-20 \leqslant k \leqslant 18$	$-23 \leqslant k \leqslant 24$
	$-18 \leqslant l \leqslant 19$	$-21 \leqslant l \leqslant 17$
Measured reflections	10,808	15,758
Reflections with $I > 3\sigma$	3243	4177
Independent reflections with $I > 3\sigma$	2197	3212
μ (mm^{-1})	4.192	3.156
Extinction coefficient g (type I, Lorentzian)	0.32×10^{-4}	0.11×10^{-4}
3—*Structure solution and refinement*		
Parameters refined	139	137
Agreement factors	$R = 0.0371$	$R = 0.0314$
	$R_w = 0.0324$	$R_w = 0.0318$
Weighting scheme	$w = 1/(\sigma^2(F) + 1 \times 10^{-4}F^2)$	$w = 1/(\sigma^2(F) + 1 \times 10^{-4}F^2)$
Δ/σ_{max}	2×10^{-4}	3×10^{-4}

For $CsAl_3(P_3O_{10})_2$, the studied crystal presented the observed systematic extinction conditions $hkl : h + k = 2n + 1$, $hk0 : h = 2n + 1$, $k = 2n + 1$ and $h0l : l = 2n + 1$, which are consistent either with the centrosymmetric space group *Cmce* (# 64) or the non-centrosymmetric space group *C2ce* (# 41). The structure was solved in the non-centrosymmetric *C2ce* space group. The structure of $CsAl_3(P_3O_{10})_2$ was determined using the heavy atom method and successive difference synthesis and Fourier synthesis. Absorption and secondary extinction effect corrections were applied. The refinement of the atomic coordinates and of the anisotropic thermal parameters of all atoms lead to the reliability factors $R = 0.0314$ and $R_w = 0.0318$ (Table 1) and to the atomic parameters listed in Table 2b.

Further details of the crystal structure investigations (including the anisotropic thermal parameters) can be obtained from the Fachinformationszentrum Karlsruhe, 76344 Eggenstein-Leopoldshafen, Germany, (fax: (49) 7247-808-666; e-mail: crysdata@fiz-karlsruhe.de) on quoteing the depository number CSD-414552 and CSD-414553 for $RbAl_3(P_3O_{10})_2$ and $CsAl_3(P_3O_{10})_2$ respectively.

3. Results and discussion

Both aluminophosphates exhibit a 3D framework $[Al_3P_6O_{20}]_\infty$ built up of corner sharing AlO_6 octahedra, AlO_4 tetrahedra and triphosphate P_3O_{10} groups, forming intersecting tunnels. Though closely related, these structures are significantly different.

3.1. Description of the $RbAl_3(P_3O_{10})_2$ host-lattice

The projections of the structure along [001] (Fig. 1) and along [110] (Fig. 2) show that the triphosphate groups and the AlO_4 and AlO_6 polyhedra form six-sided tunnels running along [001] and [110], respectively, and that the rubidium cations sit at the intersection of these

Table 2
Positional parameters, atomic displacement parameters and their estimated standard deviations

Atom	x	y	z	U_{eq} (Å^2)
a: in $RbAl_3(P_3O_{10})_2$				
Rb	−0.52329(5)	0	0	0.02464(17)
Al(1)	−0.13193(12)	0	0	0.0061(3)
Al(2)	−0.5	0.25240(11)	0.25	0.0045(3)
Al(3)	0	0.29253(11)	0.25	0.0049(3)
P(1)	−0.05324(7)	0.20594(7)	0.48905(7)	0.00509(18)
P(2)	−0.22990(8)	0.13540(6)	0.31786(7)	0.00450(18)
P(3)	−0.26395(8)	0.43193(7)	0.27694(7)	0.00445(18)
O(1)	−0.0344(2)	0.10908(18)	0.0163(2)	0.0105(6)
O(2)	−0.4267(2)	0.2522(2)	0.1043(2)	0.0082(6)
O(3)	−0.0109(2)	0.28865(18)	0.40741(18)	0.0070(5)
O(4)	−0.2010(2)	0.16449(19)	0.4452(2)	0.0074(6)
O(5)	−0.3788(2)	0.14527(18)	0.29718(19)	0.0072(6)
O(6)	−0.1359(2)	0.19081(18)	0.2423(2)	0.0078(6)
O(7)	−0.1912(2)	0.01525(18)	0.3169(2)	0.0080(6)
O(8)	−0.2549(2)	0.4923(2)	0.38780(19)	0.0087(6)
O(9)	−0.3730(2)	0.35317(19)	0.2858(2)	0.0085(6)
O(10)	−0.1278(2)	0.39658(18)	0.2386(2)	0.0093(6)
b: in $CsAl_3(P_3O_{10})_2$				
Cs	0	0	0	0.04132(12)
Al(1)	0.38030(11)	0	0	0.0078(2)
Al(2)	0.04897(8)	0.27177(5)	0.22074(5)	0.00594(13)
P(1)	0.06637(7)	0.18662(4)	0.45755(4)	0.00696(11)
P(2)	0.27095(7)	0.13268(4)	0.30481(4)	0.00610(10)
P(3)	0.30196(7)	0.42303(4)	0.28026(4)	0.00578(10)
O(1)	0.4779(2)	0.09478(14)	0.05100(15)	0.0178(5)
O(2)	0.0754(2)	0.27257(13)	0.07056(13)	0.0129(4)
O(3)	0.02893(19)	0.26411(12)	0.37393(13)	0.0115(4)
O(4)	0.21492(18)	0.14669(14)	0.42647(13)	0.0124(4)
O(5)	0.40153(19)	0.18446(13)	0.29995(15)	0.0137(4)
O(6)	0.16377(17)	0.15673(11)	0.22457(13)	0.0084(3)
O(7)	0.2982(2)	0.01604(11)	0.30423(14)	0.0133(4)
O(8)	0.2702(2)	0.46579(13)	0.39448(13)	0.0113(4)
O(9)	0.19889(19)	0.35296(13)	0.24079(15)	0.0128(4)
O(10)	0.44298(18)	0.38607(12)	0.27795(14)	0.0112(4)

All atoms were refined anisotropically and are given in the form of the isotropic equivalent displacement parameter U_{eq} defined by $U_{eq} = \frac{1}{3}\sum_{i=1}^{3}\sum_{j=1}^{3} U_{ij}a^{*i}a^{*j}\vec{a}_i\vec{a}_j$.

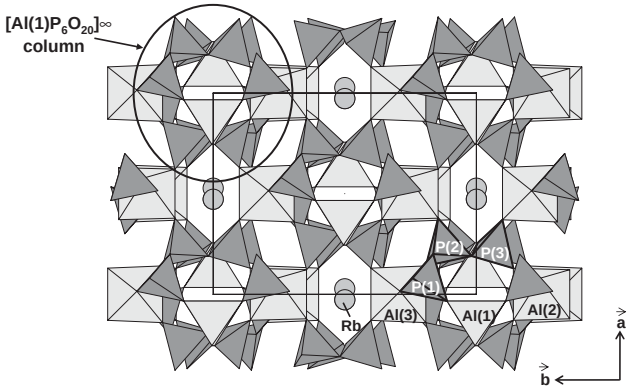

Fig. 1. Projection along [001] of the structure of $RbAl_3(P_3O_{10})_2$.

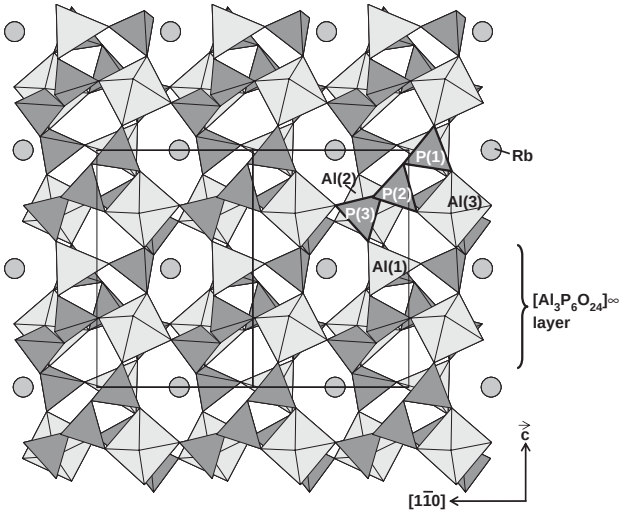

Fig. 2. Projection along [110] of the structure of $RbAl_3(P_3O_{10})_2$.

tunnels. Note that, similarly, six-sided tunnels run along [1$\bar{1}$0], which intersect the two other types of tunnels at the Rb^+ site. But the most important characteristic of this structure deals with the fact that the AlO_4 tetrahedra share their vertices with the triphosphate groups, forming isolated $[AlP_6O_{20}]_\infty$ tetrahedral columns running along $\vec{c}$ (Fig. 1). The perspective view of these columns along [010] (Fig. 3a) shows that they exhibit a helical character. One $[AlP_6O_{20}]_\infty$ tetrahedral column can indeed be described as the interlacement of two $[AlP_3O_{12}]_\infty$ helical chains around the 2_1 screw axis parallel to the $\vec{c}$ direction. In each chain, one AlO_4 alternates with one P_3O_{10} group, and two chains share their AlO_4 tetrahedra to form the $[AlP_6O_{20}]_\infty$ tetrahedral columns. The entire $[Al_3P_6O_{20}]_\infty$ framework results from the assembly of helical $[AlP_6O_{20}]_\infty$ columns of tetrahedra through AlO_6 octahedra (Fig. 1).

3.2. Description of the $CsAl_3(P_3O_{10})_2$ host-lattice

The projections of the structure of this phase along [001] (Fig. 4) and along [110] (Fig. 5) show that, like in $RbAl(P_3O_{10})_2$, the triphosphate groups share their apices with AlO_4 and AlO_6 polyhedra. However, differently from $RbAl(P_3O_{10})_2$, the P_3O_{10} and AlO_4 species do not form isolated columns, but tetrahedral $[AlP_6O_{20}]_\infty$ layers parallel to the (100) plane (Fig. 4). The perspective view of such a tetrahedral $[AlP_6O_{20}]_\infty$ layer (Fig. 6a) shows that it also presents some helical elements: two P_3O_{10} groups and one AlO_4 tetrahedron are indeed connected to form $[AlP_6O_{22}]$ helical groups (Fig. 6b). Each AlO_4 tetrahedron of one helical $[AlP_6O_{22}]$ group is linked to two other $[AlP_6O_{22}]$ groups to form the $[AlP_6O_{20}]_\infty$ tetrahedral layer. Note that similar $[AlP_6O_{22}]$ groups are observed in the $[AlP_6O_{20}]_\infty$ tetrahedral columns described above for $RbAl_3(P_3O_{10})_2$.

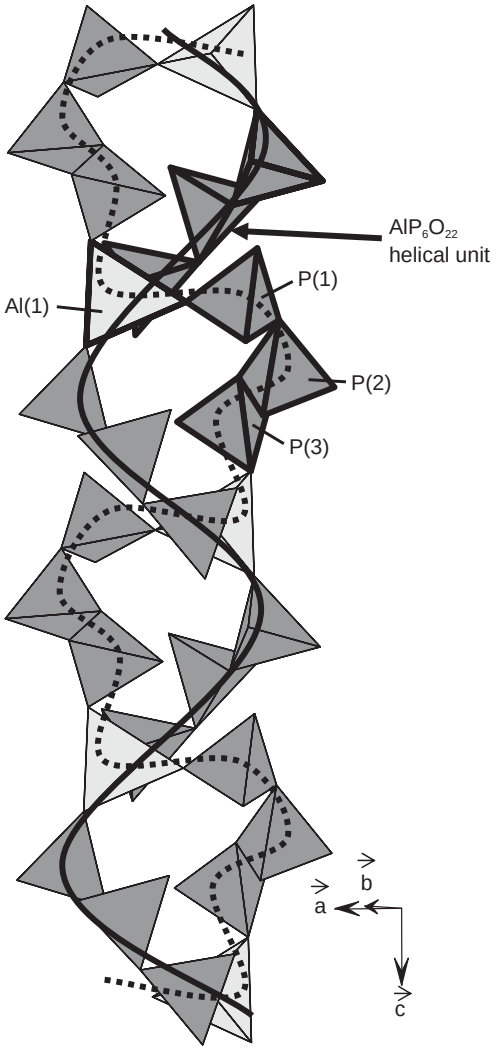

Fig. 3. Perspective view showing the helical character of the $[AlP_6O_{20}]_\infty$ tetrahedral column running along the [001] direction in $RbAl_3(P_3O_{10})_2$. The two interlaced $[AlP_3O_{12}]_\infty$ chains are shown (continuous and dotted lines). One $[AlP_6O_{22}]$ tetrahedral building unit of the $[AlP_6O_{20}]_\infty$ column is emphasized (bold lines).

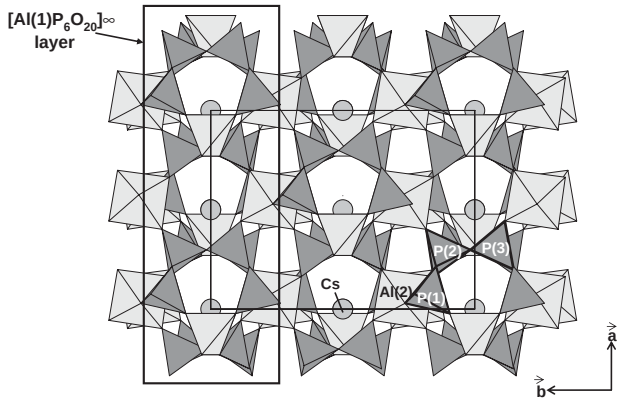

Fig. 4. Projection along [001] of the structure of $CsAl_3(P_3O_{10})_2$.

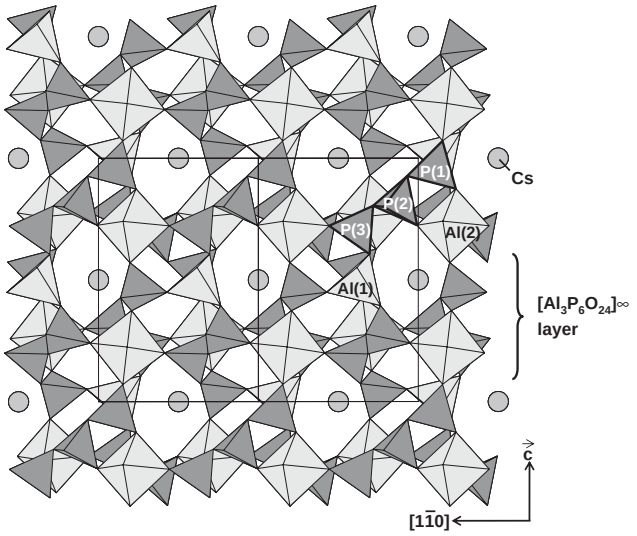

Fig. 5. Projection along [110] of the structure of $CsAl_3(P_3O_{10})_2$.

Nevertheless, in these columns two successive $[AlP_6O_{22}]$ units are deduced one from the other through the 2_1 screw axis parallel to the [001] direction (Fig. 3), whereas the $[AlP_6O_{22}]$ units are related through the *n* glide mirror in a $[AlP_6O_{20}]_\infty$ layer. The entire $[Al_3P_6O_{20}]_\infty$ framework results from the association of the $[AlP_6O_{20}]_\infty$ tetrahedral layers through single AlO_6 octahedra (Fig. 4). The 3D $[Al_3P_6O_{20}]_\infty$ framework delimits also intersecting tunnels running along the [001] and $\langle 110 \rangle$ directions (Figs. 4 and 5) and the Cs^+ cations sit at the intersections of these tunnels. The shape of the six-sided $\langle 110 \rangle$ tunnels (Fig. 5) is rather similar to that observed in the Rb-phase, whereas the five-sided [001] tunnels of the Cs-phase (Fig. 4) are very different from the six-sided [001] tunnels of the Rb-phosphate (Fig. 1).

3.3. *Relationships between the $RbAl_3(P_3O_{10})_2$ and $CsAl_3(P_3O_{10})_2$ host-lattices*

In spite of the different arrangements of their AlO_4 and PO_4 tetrahedra, the $[Al_3P_6O_{20}]_\infty$ 3D frameworks of these two triphosphates exhibit close relationships. The latter are clearly evidenced by comparing the projections of these structures along [110] (Figs. 2 and 5). One indeed observes that each of these structures can be described by the stacking along $\vec{c}$ of identical $[Al_3P_6O_{24}]_\infty$ layers. The projections of these $[Al_3P_6O_{24}]_\infty$ layers along $\vec{c}$ show their great similarity. In both cases, Rb-phase (Fig. 7a) and Cs-phase (Fig. 7b), the AlO_6 octahedra are displayed on an approximately square array and joined through PO_4 tetrahedra to form $[Al_2P_4O_{22}]$ rings, which are overhung by $[AlP_2O_{10}]$ bridges. Thus, similar six-sided, five-sided and diamond-shape windows are observed for the two types of layers. The main difference between these two layers deals with the configuration of the $[Al_2P_4O_{22}]$ rings and

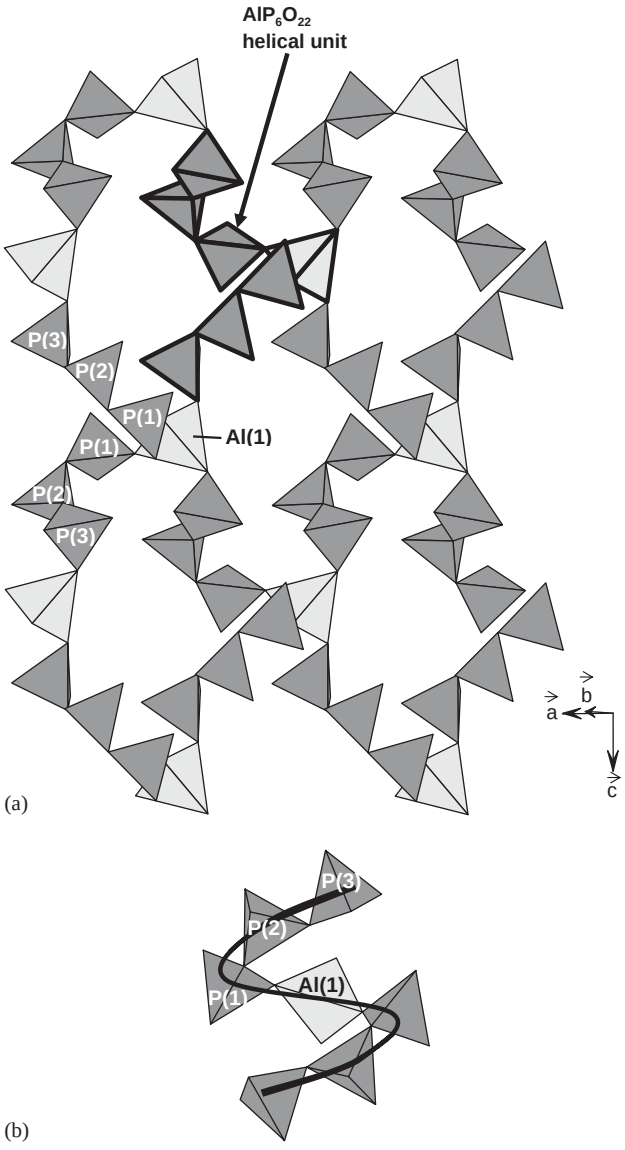

Fig. 6. (a) Perspective view of one $[AlP_6O_{20}]_\infty$ tetrahedral layer parallel to the (100) plane, showing its helicoïdal character. (b) The "AlP_6O_{22}" helical unit encountered in the $[AlP_6O_{20}]_\infty$ tetrahedral layers of $CsAl_3(P_3O_{10})_2$ and in the $[AlP_6O_{20}]_\infty$ tetrahedral columns of $RbAl_3(P_3O_{10})_2$.

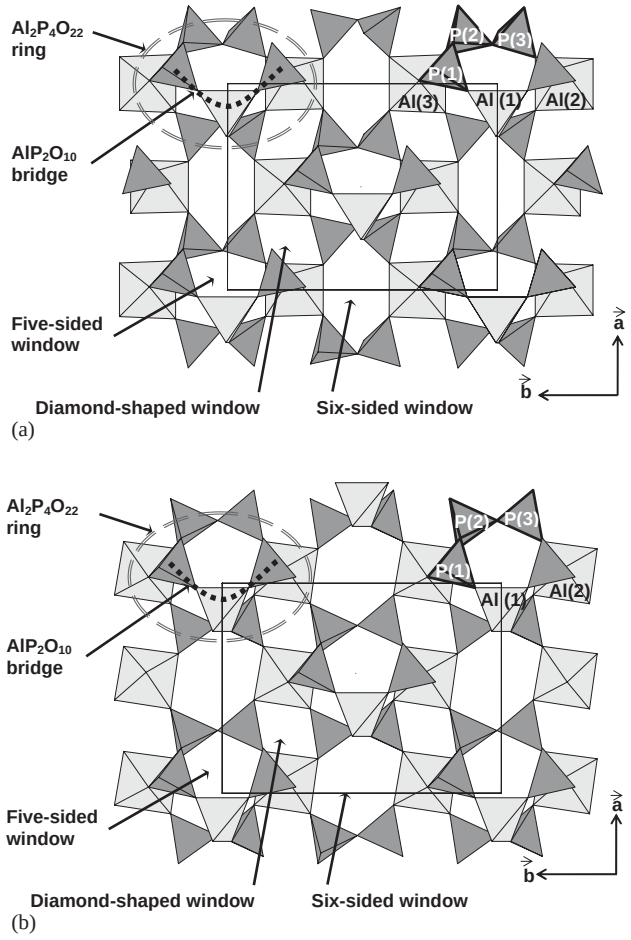

Fig. 7. Projection of one $[Al_3P_6O_{24}]_\infty$ layer parallel to the (001) plane observed (a) in $RbAl_3(P_3O_{10})_2$ and (b) in $CsAl_3(P_3O_{10})_2$.

$[AlP_2O_{10}]$ bridges, which make that the windows are significantly more opened in the Cs–triphosphate (Fig. 7b) than in the Rb–triphosphate (Fig. 7a). The stacking of the $[Al_3P_6O_{24}]_\infty$ layers along $\vec{c}$ in the Rb-phase is thus different from the one observed in the Cs-phase: two successive layers are deduced one from the other by 2_1 screw axis in the first one (Fig. 2), whereas they correspond through a c glide mirror in the second one (Fig. 5). Due to these different stacking modes, one observes twice more five-sided tunnels running along $\vec{c}$ in the Cs-phosphate (Fig. 4), than six-sided tunnels along that direction in the Rb-phosphate (Fig. 1). Moreover, the $\langle 110 \rangle$ tunnels are aligned along the $\vec{c}$ direction in the Rb-phase (Fig. 2), whereas they form staggered rows along that direction in the Cs-phase (Fig. 5).

3.4. Comparison with other triphosphates

One important characteristic of these two compounds deals with the fact that their framework is built up of triphosphate groups. The latter seems to be currently observed in phosphates involving hydroxyl groups and water molecules. In contrast, only nine different types of "non-containing hydrogen atoms" host-lattices with triphosphate groups have been synthesized to date to our knowledge. Five of them contain only P_3O_{10} groups: $ABe_2P_3O_{10}$ ($A = Rb$, NH_4) [12,13], $KThP_3O_{10}$ [14], $Na_5P_3O_{10}$ [15–17], $LiM_2P_3O_{10}$ ($M = Co$, Ni) [18,19] and $CsMP_3O_{10}$ with $M = Ga$, Al, Cr [7]. The four others can be described as mixed phosphates containing simultaneously P_3O_{10} and PO_4 groups as in $U_2P_3O_{10}(PO_4)$ [20] and $CsTa_2P_3O_{10}(PO_4)_2$ [21] or P_3O_{10} and P_2O_7 groups as in $Na_7Y_2P_3O_{10}(P_2O_7)_2$ [22] and $AM_6P_3O_{10}(P_2O_7)_2$ with $A = NH_4$, K, Na, Ag and $M = Cd$, Mn [23,24]. Remarkably, $RbAl_3(P_3O_{10})_2$

Table 3a
Bond distances (Å) and angles (deg) in $RbAl_3(P_3O_{10})_2$

Al(1)	O(1)	O(1^{i})	O(8^{ii})	O(8^{iii})
O(1)	**1.715(2)**	2.838(4)	2.895(3)	2.811(3)
O(1^{i})	111.69(12)	**1.715(2)**	2.811(3)	2.895(3)
O(8^{ii})	113.56(11)	108.62(11)	**1.746(2)**	2.682(3)
O(8^{iii})	108.62(11)	113.56(11)	100.37(11)	**1.746(2)**

Al(2)	O(2)	O(2^{iv})	O(5)	O(5^{iv})	O(9)	O(9^{iv})
O(2)	**1.882(2)**	3.763(3)	2.722(3)	2.639(5)	2.580(3)	2.706(3)
O(2^{iv})	179.84(14)	**1.882(2)**	2.639(5)	2.722(3)	2.706(3)	2.580(3)
O(5)	91.70(10)	88.18(10)	**1.911(3)**	2.645(3)	2.683(4)	3.763(3)
O(5^{iv})	88.18(10)	91.70(10)	87.56(11)	**1.911(3)**	3.763(3)	2.683(4)
O(9)	87.31(10)	92.80(11)	90.83(10)	175.17(10)	**1.855(3)**	2.650(3)
O(9^{iv})	92.80(11)	87.31(10)	175.17(10)	90.83(10)	91.13(12)	**1.855(3)**

Al(3)	O(3)	O(3^{v})	O(6)	O(6^{v})	O(10)	O(10^{v})
O(3)	**1.880(2)**	3.758(3)	2.643(3)	2.622(3)	2.705(3)	2.616(3)
O(3^{v})	176.94(14)	**1.880(2)**	2.622(3)	2.643(3)	2.616(3)	2.705(3)
O(6)	89.38(10)	88.48(10)	**1.878(3)**	2.691(3)	2.653(4)	3.724(3)
O(6^{v})	88.48(10)	89.38(10)	91.50(11)	**1.878(3)**	3.724(3)	2.653(4)
O(10)	93.08(11)	89.15(11)	90.85(10)	177.19(11)	**1.847(3)**	2.539(3)
O(10^{v})	89.15(11)	93.08(11)	177.19(11)	90.85(10)	86.84(11)	**1.847(3)**

P(1)	O(1^{v})	O(2^{vi})	O(3)	O(4)
O(1^{v})	**1.520(3)**	2.528(3)	2.525(4)	2.476(3)
O(2^{vi})	114.32(14)	**1.489(3)**	2.483(3)	2.518(3)
O(3)	113.35(13)	112.20(15)	**1.502(3)**	2.508(3)
O(4)	103.08(13)	107.06(12)	105.79(13)	**1.640(2)**

P(2)	O(4)	O(5)	O(6)	O(7)
O(4)	**1.589(3)**	2.501(3)	2.526(3)	2.458(4)
O(5)	108.24(13)	**1.496(2)**	2.555(3)	2.509(3)
O(6)	110.84(13)	118.43(14)	**1.477(2)**	2.490(4)
O(7)	101.13(13)	108.50(13)	108.30(13)	**1.594(3)**

P(3)	O(7^{vii})	O(8)	O(9)	O(10)
O(7^{vii})	**1.613(3)**	2.515(3)	2.503(4)	2.444(3)
O(8)	105.98(14)	**1.536(3)**	2.460(3)	2.502(3)
O(9)	107.79(13)	109.11(13)	**1.483(2)**	2.458(3)
O(10)	103.79(13)	111.45(13)	117.88(14)	**1.491(2)**

Rb–O(3^{ii})	2.958(3)
Rb–O(3^{iii})	2.958(3)
Rb–O(5^{viii})	3.207(2)
Rb–O(5^{iv})	3.207(2)
Rb–O(8^{ii})	3.057(2)
Rb–O(8^{iii})	3.057(2)
Rb–O(10^{ix})	3.306(2)
Rb–O(10^{x})	3.306(2)

Symmetry codes
(i) $x, -y, -z$, (ii) $-\frac{1}{2}-x, \frac{1}{2}-y, -\frac{1}{2}+z$, (iii) $-1-x, -1+y, \frac{1}{2}-z$, (iv) $-\frac{1}{2}-x, \frac{1}{2}+y, \frac{1}{2}-z$, (v) $\frac{1}{2}-x, \frac{1}{2}+y, \frac{1}{2}-z$, (vi) $-\frac{1}{2}-x, \frac{1}{2}-y, \frac{1}{2}+z$, (vii) $-1-x, y, \frac{1}{2}-z$, (viii) $-1-x, -y, -\frac{1}{2}+z$, (ix) $-\frac{1}{2}+x, -\frac{1}{2}+y, z$, (x) $-\frac{1}{2}+x, \frac{1}{2}-y, -z$.

and $CsAl_3(P_3O_{10})_2$ are the only triphosphates, with $ABe_2P_3O_{10}$ compounds [12,13] whose P_3O_{10} groups share corners with other tetrahedra, i.e., AlO_4 or BeO_4 species. It is also worth to emphasize that this association of P_3O_{10} and AlO_4 tetrahedra leads to the formation of 1D (helical $[AlP_6O_{20}]_\infty$ columns) or 2D

Table 3b
Bond distances (Å) and angles (deg) in $CsAl_3(P_3O_{10})_2$

Al(1)	O(1)	O(1^{i})	O(8^{ii})	O(8^{iii})
O(1)	**1.7113(17)**	2.8108(19)	2.775(3)	2.932(2)
O(1^{i})	110.42(10)	**1.7113(17)**	2.932(2)	2.775(3)
O(8^{ii})	106.52(7)	115.68(7)	**1.7518(17)**	2.7242(17)
O(8^{iii})	115.68(7)	106.52(7)	102.08(10)	**1.7518(17)**

Al(2)	O(2)	O(3)	O(5^{iv})	O(6)	O(9)	O(10^{iv})
O(2)	**1.8462(14)**	3.7220(17)	2.623(3)	2.5828(19)	2.638(2)	2.726(2)
O(2^{iv})	176.54(8)	**1.8775(14)**	2.688(3)	2.677(2)	2.630(2)	2.6056(19)
O(5)	89.04(10)	90.90(10)	**1.8943(19)**	2.667(3)	3.758(3)	2.7266(19)
O(5^{iv})	86.74(7)	89.79(7)	88.90(8)	**1.9142(18)**	2.6418(19)	3.767(2)
O(9)	90.63(7)	89.29(7)	177.59(8)	88.70(8)	**1.8646(19)**	2.608(3)
O(9^{iv})	94.89(7)	88.58(7)	93.34(8)	177.25(8)	89.07(8)	**1.8539(17)**

P(1)	O(1^{iv})	O(2^{v})	O(3)	O(4)
O(1^{iv})	**1.5119(17)**	2.500(2)	2.4832(19)	2.485(3)
O(2^{v})	113.29(9)	**1.4816(13)**	2.4870(18)	2.485(2)
O(3)	111.28(9)	113.26(8)	**1.4963(14)**	2.512(2)
O(4)	104.82(9)	106.27(10)	107.24(9)	**1.623(2)**

P(2)	O(4)	O(5)	O(6)	O(7)
O(4)	**1.5945(14)**	2.471(3)	2.5132(18)	2.435(2)
O(5)	107.04(12)	**1.478(2)**	2.576(3)	2.468(2)
O(6)	109.36(10)	120.78(11)	**1.4846(18)**	2.500(2)
O(7)	100.39(7)	107.83(10)	109.50(9)	**1.5757(15)**

P(3)	O(7)	O(8)	O(9)	O(10)
O(7)	**1.6084(14)**	2.5242(18)	2.447(2)	2.467(2)
O(8)	106.79(7)	**1.5354(14)**	2.5017(19)	2.747(2)
O(9)	105.18(9)	112.66(10)	**1.4702(18)**	2.523(3)
O(10)	105.25(9)	109.51(9)	116.62(9)	**1.494(2)**

Cs–O(3^{ii})	3.5048(13)
Cs–O(3^{iii})	3.5048(13)
Cs–O(4^{iv})	3.5698(18)
Cs–O(4^{vii})	3.5698(18)
Cs–O(5^{iv})	3.594(2)
Cs–O(5^{vii})	3.594(2)
Cs–O(7^{iv})	3.1304(16)
Cs–O(7^{vii})	3.1304(16)
Cs–O(8^{ii})	3.0271(19)
Cs–O(8^{iii})	3.0271(19)

Symmetry codes
(i) $x, -y, -z$, (ii) $x, -\frac{1}{2}+y, \frac{1}{2}-z$, (iii) $\frac{1}{2}+x, 1-y, -\frac{1}{2}+z$, (iv) $-\frac{1}{2}+x, -1+y, \frac{1}{2}-z$, (v) $\frac{1}{2}+x, 1-y, \frac{1}{2}+z$, (vi) $x, \frac{1}{2}+y, \frac{1}{2}-z$, (vii) $-1+x, -\frac{3}{2}-y, -\frac{1}{2}+z$.

(helicoïdal $[AlP_6O_{20}]_\infty$ layers) tetrahedral frameworks, whereas a 3D-tetrahedral framework built up of BeO_4 and P_3O_{10} species is obtained for $A Be_2P_3O_{10}$ phases. This different behaviour of aluminium triphosphates compared to the beryllium triphosphates is easily explained by the ability of aluminium to adopt both tetrahedral and octahedral coordinations. The presence in the same framework of two different kinds of polyhedra for aluminium together with triphosphates is also a remarquable feature. Most of the non-organically templated and non-fluorinated phosphates presenting such structural characteristic contain water molecules and/or hydroxyl groups. To our knowledge, there are only two ''non-containing hydrogen atoms'' aluminium phosphates with this characteristic: $Mg_6Si_2Al_{22}P_{26}O_{112}$, with aluminium atoms in octahedral and tetrahedral coordinations [25] and $NaRb_2Al_2(PO_4)_3$, involving AlO_4 and AlO_5 polyhedra [8].

3.5. Configuration of the P_3O_{10} groups and interatomic distances

The previous studies of the triphosphates have shown the great flexibility of the P_3O_{10} groups, whose geometry depends on the mode of connection of the latter with the surrounding octahedra and tetrahedra.

In the two present phases, both P_3O_{10} groups exhibit a similar geometry. The average values for the P–P distances (2.88 Å) and the P–P–P angles (124°) are intermediate between the limit values observed in the literature for triphosphate groups in different compounds. One generally observes P–P distances ranging from 2.76 to 3.05 Å, whereas the P–P–P angles may vary from 80° when the P_3O_{10} group share three apices with the same octahedron, to 151° when each PO_4 tetrahedron is linked to a different coordination polyhedron of the framework [7,15–17,26]. In the present phases, the fact that each P_2O_7 group belonging to the P_3O_{10} groups shares two apices with the same AlO_6 octahedron induces P–P–P angles smaller than 151°, i.e., of ca. 124°.

The geometry of the PO_4 tetrahedra is close to that generally observed. Two groups of distances can be distinguished. The P–O bonds corresponding to the two P–O–P bridges of the P_3O_{10} groups are the largest one (ranging from 1.5757(15) to 1.640(2) Å) (Table 3). Consequently, the two "external" tetrahedra P(1) and P(3) present one long P–O distance (from 1.6084(14) to 1.640(2) Å) and three smaller ones (from 1.4702(18) to 1.536(3) Å), whereas the "central" P(2) tetrahedron has two long P–O distances (from 1.5757(15) to 1.5945(14) Å) and two shorter ones (from 1.477(2) to 1.4963(14) Å) (Table 3).

The AlO_4 and AlO_6 polyhedra are quite regular with Al–O distances ranging from 1.7113(17) to 1.7518(17) Å in the Al tetrahedra, and from 1.8462(14) to 1.9142(18) in the Al octahedra.

The rubidium cations exhibit an eight-fold coordination with Rb–O distances ranging from 2.958(3) to 3.306(2) Å (Table 3a), whereas the cesium cations are environed by ten oxygen atoms with significantly longer Cs–O distances, ranging from 3.0271(19) to 3.594(2) Å (Table 3b).

4. Conclusion

Aluminophosphates involving simultaneously triphosphate groups, AlO_4 tetrahedra and AlO_6 octahedra have been synthesized for the first time. More importantly, this study shows the exceptional ability of such aluminotriphosphates to form 1D and 2D "Al–P–O" tetrahedral frameworks with an original helical geometry. This suggests that numerous "Al–P–O" tetrahedral frameworks remain to be discovered and that it should be possible to control their dimensionality by the introduction of AlO_6 octahedra.

Acknowledgments

Authors want to thank Drs. O. Pérez and S. Marinel for their friendly collaboration to this work.

This work is supported by the Région Basse Normandie and the Ministère de la Recherche.

References

[1] M.E. Davis, Chem. Eur. J. 3 (11) (1997) 1745–1750.
[2] A.K. Cheetham, G. Férey, T. Loiseau, Angew. Chem. Int. Ed. 38 (1999) 3268–3292.
[3] M.E. Davis, I.E. Maxwell, Curr. Opin. Solid State Mater. Sci. 1 (1996) 55–56.
[4] I.E. Maxwell, P.W. Lednor, Curr. Opin. Solid State Mater. Sci. 1 (1996) 57–64.
[5] G.J. Mc Carthy, W.B. White, D.E. Pfoertsch, Mater. Res. Bull. 13 (1978) 1239.
[6] J. Carpéna, J.L. Lacout, L'Actualité Chim. 2 (1997) 3.
[7] A. Guesdon, E. Daguts, B. Raveau, J. Solid State Chem. 167 (2002) 258–264.
[8] Q. Huang, S.-J. Hwu, Chem. Mater. 13 (2001) 1794–1799.
[9] J. Rodriguez-Carvajal, FULLPROF: A Program for Rietveld Refinement and Pattern Matching Analysis, Abstracts of the Satellite Meeting on Powder Diffraction of the XV Congress of the IUCr, Toulouse, France, 1990, p. 127.
[10] Duisenberg, Kroon-Batenburg, Schreurs, J. Appl. Cryst. 36 (2003) 220.
[11] V. Pretricek, M. Dusek, The crystallographic computing system JANA2000, Institute of Physics, Praha, Czech Republic, 2000.
[12] M.T. Averbuch-Pouchot, A. Durif, C. R. Acad. Sci., Séries 2 316 (1993) 609–614.
[13] M.T. Averbuch-Pouchot, A. Durif, J. Coing-Boyat, J.C. Guitel, Acta Crystallogr. B 33 (1977) 203–205.
[14] Z. Ruzic Toros, B. Kojic-Prodic, R. Liminga, S. Popovic, Inorg. Chim. Acta 8 (1974) 273–278.
[15] D.E.C. Corbridge, Acta Crystallogr. 13 (1960) 263–269.
[16] R. Davies, D.E.C. Corbridge, Acta Crystallogr. 11 (1958) 315–319.
[17] D.W.J. Cruickshank, Acta Crystallogr. 17 (1964) 674–675.
[18] F. Erragh, A. Boukhari, E.M. Holt, Acta Crystallogr. C 52 (1996) 1867–1869.
[19] K. Rissouli, K. Benkhouja, A. Sadel, M. Bettach, M. Zahir, Eur. J. Solid State Inorg. Chem. 34 (1997) 221–230.
[20] R. Podor, M. Francois, N. Dacheux, J. Solid State Chem. 172 (2003) 66–72.
[21] G.G. Sadikov, V.P. Nikolaev, A.V. Lavrov, M.A. Porai-Koshits, Doklady Akad. Nauk SSSR 264 (1982) 862–867.
[22] A. Hamady, T. Jouini, Z. Anorg. Allg. Chem. 622 (1996) 1987–1990.
[23] J. Bennazha, A. ElMaadi, A. Boukhari, E.M. Holt, Solid State Sci. 3 (2001) 587–592.
[24] J. Bennazha, A. ElMaadi, A. Boukhari, E.M. Holt, Acta Crystallogr. C 58 (2002) i76–i78.
[25] J.M. Bennett, B.K. Marcus, Stud. Surf. Sci. Catal. 38 (1988) 269–279.
[26] M.T. Averbuch-Pouchot, A. Durif, Topics in Phosphate Chemistry, World Scientific, Singapore, 1996, p. 177.